ISSN : 0974 - 7524 Volume 9 Issue 6

Physical CHEMISTRY
An Indian Journal

Full Paper

PCAIJ, 9(6), 2014 [205-210]

Structural characterization and oxide ionic conductivity of new silicate oxyapatite $La_{9.13}Bi_{0.2}(SiO_4)_6O_2$

Mohamed Abbassi[1], Riadh Ternane[1]*, Malika Trabelsl-Ayadi[1], Jesus Sanz[2]

[1]Laboratoire d'Application de la Chimie aux Ressources et Substances Naturelles et à l'Environnement (LACReSNE), Université de Carthage, Faculté des Sciences de Bizerte, 7021 Zarzouna, Bizerte, (TUNISIA)

[2]Instituto de Ciencia de Materiales de Madrid (ICMM), Consejo Superior de Investigaciónes Científicas (CSIC), Cantoblanco, 28049 Madrid, (SPAIN)

E-mail : rternane@yahoo.fr

ABSTRACT

New bismuth oxyapatite $La_{9.13}Bi_{0.2}(SiO_4)_6O_2$ has prepared by the solid-state reaction. X-ray diffraction, FTIR spectroscopy, Raman scattering spectroscopy and SEM-EDS techniques have been used in the characterization of this sample. The average crystalline size has been calculated using the Scherrer formula and it is found to be ~37 nm.

Impedance analysis indicated the negative temperature coefficient of resistance (NTCR) behaviour of $La_{9.13}Bi_{0.2}(SiO_4)_6O_2$. The ionic conductivity is equal to 1.46×10^{-4} S.cm^{-1} at 973 K with activation energy of 0.84 eV.

KEYWORDS

Oxyapatite;
XRD;
Raman;
SEM-EDS;
Ionic conduction,
SOFC.

INTRODUCTION

Solid Oxide Fuel Cells (SOFCs) are promising solid devices for the electrochemical conversion of a fuel directly into electrical power. Recently, apatite-type silicates have been considered as promising electrolytes for SOFCs exhibiting a significant oxygen ionic conductivity and moderate thermal expansion[1-6] and have been also a low activation energy and excellent stability over a wide oxygen partial pressure range[7,8].

Silicate oxyapatites, with general formula $Me_{10}(SiO_4)_6O_2$ (space group $P6_3/m$), where Me is a metal such as rare earth or alkaline earth, are built up of isolated SiO_4 tetrahedra that share oxygens with Me polyhedra to form a rigid network. In these compounds, O (5) oxide ions, occupying the centre of one-dimensional channels running along the *c*-axis, are responsible of ionic conduction. Me cations are located in 7 and 9 coordinated sites, labeled Me_I and Me_{II} sites, respectively.

In the present work, the $La_{9.13}Bi_{0.2}(SiO_4)_6O_2$ material has synthesized by solid-state reaction. The structural characterization of prepared material has been performed with XRD, FTIR, Raman and SEM-EDS techniques and ionic transport studies like, conductivity and the relaxation behavior through impedance measurements to develop the better property solid electrolyte for intermediate temperature solid oxide fuel cell (IT-SOFC) applications.

EXPERIMENTAL

Full Paper

Sample preparation

$La_{9.13}Bi_{0.2}(SiO_4)_6O_2$ apatite has been synthesized using the solid-state reaction. The starting materials were SiO_2 (99.99 %), La_2O_3 (99 %) and Bi_2O_3 (99 %). Stoichiometric amounts of reactants have been heated in a covered platinum crucible at 1173 K for 24h and at 1523 K for 24h with intermediate grindings.

Structural characterization

X-ray diffraction (XRD) patterns have been recorded with a BRUKER D8-advance diffractometer using the CuKα radiation (λ = 1.5406 Å). The crystalline phases have been identified using the International Centre for Diffraction Data (ICDD) powder diffraction files. Cell parameters have been refined with the FULLPROF program.

Fourier transformed infrared (FTIR) spectra have been obtained with a BRUKER spectrometer, in the 4000-400 cm^{-1} range, using the KBr pellet technique. Raman spectra have been recorded at room temperature in the spectral range 100-1200 cm^{-1} in a DILOR XY spectrometer equipped with a CCD detector and a Spectra Physics Ar laser (excitation at 514.5 nm). SEM images and X-rays Energy Dispersion spectra (EDS) have been obtained using a scanning electron microscope (SEM) (FE™/NOVA NANOSEM 230).

Electrical measurements

Electrical conductivity measurements of the samples have been performed using an automatically controlled HP4192A analyzer working at 120 frequencies, log-scaled between 5 Hz and 13 MHz. In electrical measurements, a sinusoidal signal of 50 mV has been used. High temperature measurements have been performed between 673 K and 1073 K under air atmosphere. Powders have been pressed under 5 tons.cm^{-2} and sintered at 1523 K. Electrodes have been prepared by painting a Pt paste on both sides of the sintered pellet surfaces, which have been then heated at 1028 K to ensure good electrical contact.

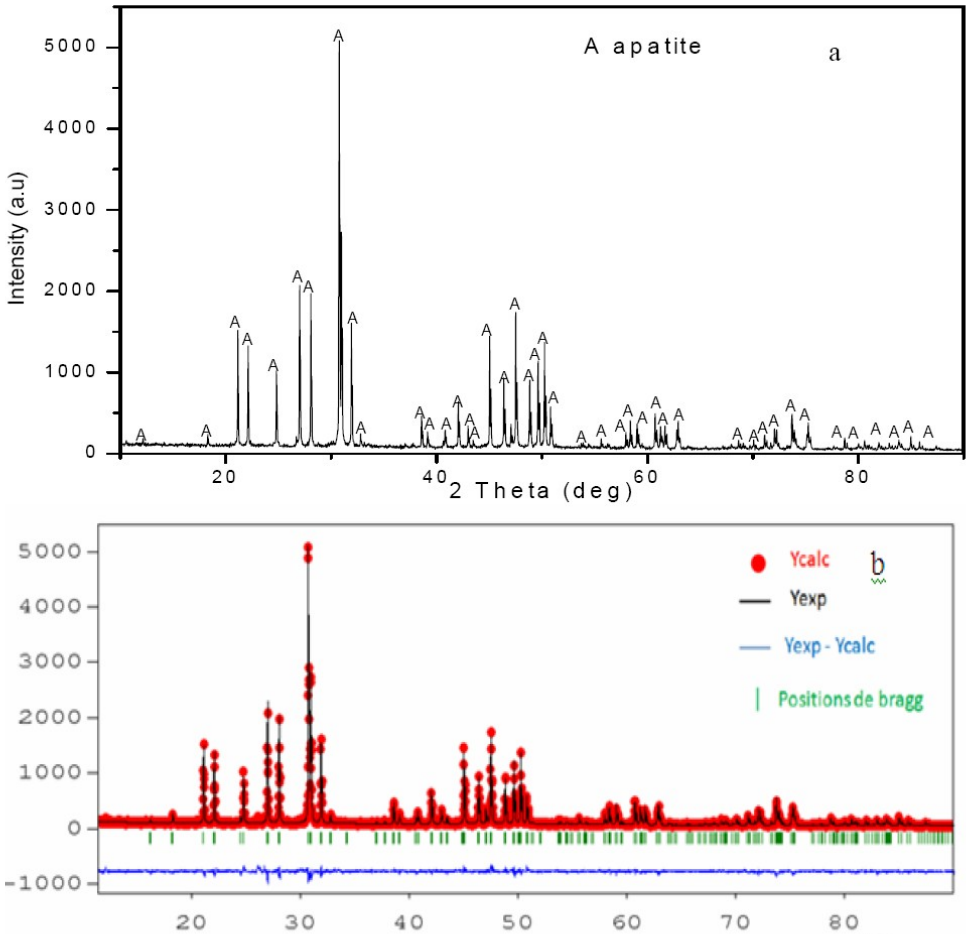

Figure 1 : (a) XRD patterns and (b) Rietveld refined patterns of $La_{9.13}Bi_{0.2}(SiO_4)_6O_2$ oxyapatite

RESULTS AND DISCUSSIONS

X-ray diffraction

The X-ray patterns of the synthesized $La_{9.13}Bi_{0.2}(SiO_4)_6O_2$ are shown in Figure 1a. All the present lines have been indexed in the hexagonal system (space group $P6_3$ (173)). The lattice parameters of the sample have been found to be a =9.7247 Å, c = 7.1904 Å, and V = 508.875 Å^3.

The structural refinement of the $La_{9.13}Bi_{0.2}(SiO_4)_6O_2$ has been carried out using the Rietveld method. The fitting of the XRD patterns of the sample is shown in Figure 1b.

It can be seen that the profiles for observed and calculated one are perfectly matching which is well supported by the value of χ^2 (= 1.48).

The crystal data and refinement factors of $La_{9.13}Bi_{0.2}(SiO_4)_6O_2$ obtained from XRD data are depicted in TABLE 1. The average crystallite size of $La_{9.13}Bi_{0.2}(SiO_4)_6O_2$ material calculated using the Scherer's formula, have been found to be ~37 nm.

TABLE 1 : Details of the Rietveld refinement of the X-ray powder diffraction patterns of $La_{9.13}Bi_{0.2}(SiO_4)_6O_2$ oxyapatite

Formula	$La_{9.13}Bi_{0.2}(SiO_4)_6O_2$
Space group symmetry	hexagonal $P6_3$
Formula units per cell Z	1
units cell dimensions	
a (Å)	9.7247
c (Å)	7.1904
R_p	20.7
R_{wp}	19.8
R_B	5.541
R_F	5.464
$\chi 2$	1.48
u, v, w	0.021856, -0.010750, 0.003578

Vibrational infrared and raman spectra

The IR spectrum of the $La_{9.13}Bi_{0.2}(SiO_4)_6O_2$ sample is shown in Figure 2a. The band assignment is summarized in table 2, according to the literature[9-11]. The bands at 994-880 cm^{-1} and 545-412 cm^{-1} ranges are attributed to the stretching (symmetric ν_s and antisymmetric ν_{as}) and bending (symmetric δ_s and antisymmetric δ_{as}) vibrational modes of isolated SiO_4 tetrahedra, respectively. The absence of bands at 3572 and 630 cm^{-1}, corresponding to stretching and libration modes of OH groups, proves that synthesized sample is not hydroxyapatite[12].

The Raman spectrum of the $La_{9.13}Bi_{0.2}(SiO_4)_6O_2$ sample is given in Figure 2b. The observed major bands can be assigned to their corresponding modes based on the related silicate apatites[13-16]. The Raman spectrum can be divided into two clearly differentiated regions, above and below 280 cm^{-1}. The Raman peaks above 280 cm^{-1} can be assigned to internal modes of the tetrahedral SiO_4 units. The intense band at 386 cm^{-1} can be assigned to the symmetric bending mode δ_s of the SiO_4 group and the one at ~ 520 cm^{-1} to the asymmetric bending mode δ_{as}. The intense band at 855 cm^{-1} is due to the symmetric stretching mode ν_s of SiO_4 tetrahedra. The weak band at ~ 930 cm^{-1} can be attributed to the asymmetric stretching mode ν_{as}. These bands confirm the presence of isolated orthosilicate groups in the prepared material. The band positions are listed in TABLE 2.

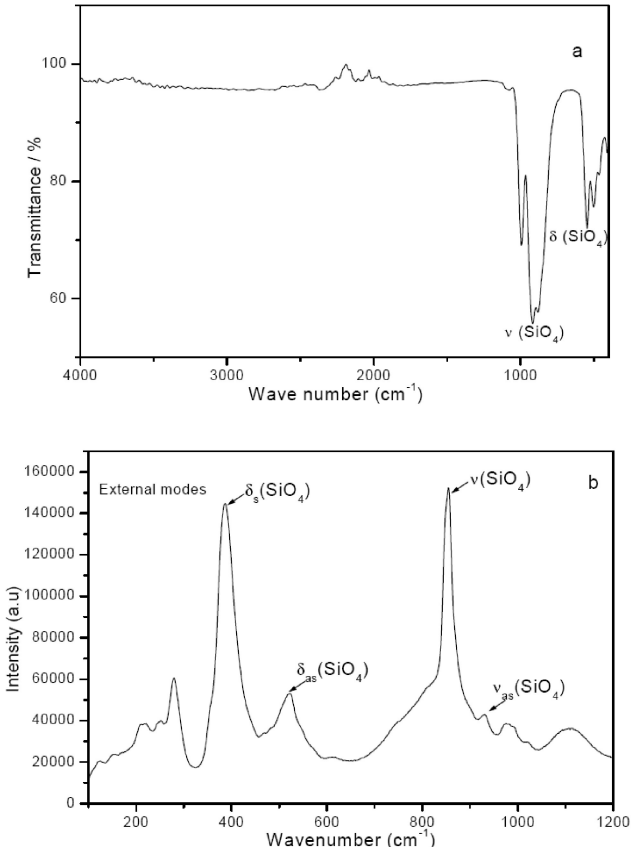

Figure 2 : (a) FTIR and (b) Raman spectra of $La_{9.13}Bi_{0.2}(SiO_4)_6O_2$ oxyapatite

Full Paper

TABLE 2 : Assignments (cm^{-1}) of FT-IR and Raman spectra of $La_{9.13}Bi_{0.2}(SiO_4)_6O_2$ oxyapatite

Compound	Infrared spectroscopy				Raman spectroscopy			
	ν_s	δ_s	ν_{as}	δ_{as}	ν_s	δ_s	ν_{as}	δ_{as}
$La_{9.13}Bi_{0.2}(SiO_4)_6O_2$	881	412	915-992	546-501	855	386	930-975	520

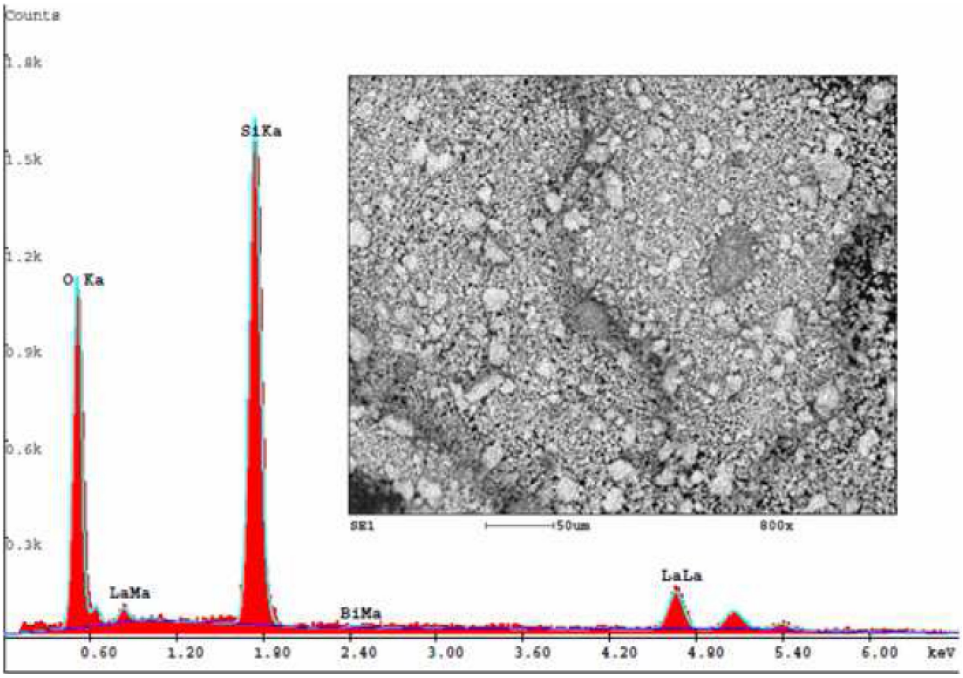

Figure 3 : EDS spectrum and SEM micrograph of $La_{9.13}Bi_{0.2}(SiO_4)_6O_2$ oxyapatite

SEM-EDS analysis

Fig.3. shows the EDS patterns and SEM micrograph (inset) of $La_{9.13}Bi_{0.2}(SiO_4)_6O_2$ sample. The peaks have perfectly assigned to the present elements in our sample. SEM-EDS results confirm the formation of exact composition of $La_{9.13}Bi_{0.2}(SiO_4)_6O_2$. Irregular shaped grains of unequal sizes distributed throughout the sample and formation of big agglomerates, are clearly visible in the SEM-micrograph. The theoretical density obtained from the lattice parameters is ~ 5.34 $g.cm^{-3}$.

Electrical characterization

Figure 4 shows complex impedance spectra (Nyquist diagrams) of $La_{9.13}Bi_{0.2}(SiO_4)_6O_2$ sample over a wide range of temperatures. There are two semicircles in each impedance spectrum with different frequencies corresponding to grain boundary R_{gb} and bulk (grain) R_b. The resistance of bulk and grain boundary could directly be obtained from the intercept on the Z'axis. The total resistivity of the electrolyte is given by $R_t = (R_b) + (R_{gb})$. Bulk conductivities σ_b and grain boundary conductivities σ_{gb} values have been estimated with the relation:

$\sigma_j = \ell/R_j S$. where R_j (j=bulk, grain boundary) is the resistance deduced from impedance diagrams, S and ℓ are the area and the thickness of pellet, respectively. It is difficult to distinguish the bulk resistance and the grain boundary resistance above 1023 K.

The total resistance decreases with rise in temperature. Thus, the total electrical conductivity of the material increases with the rise in temperature. This behavior of materials is analogous to the negative tempera-

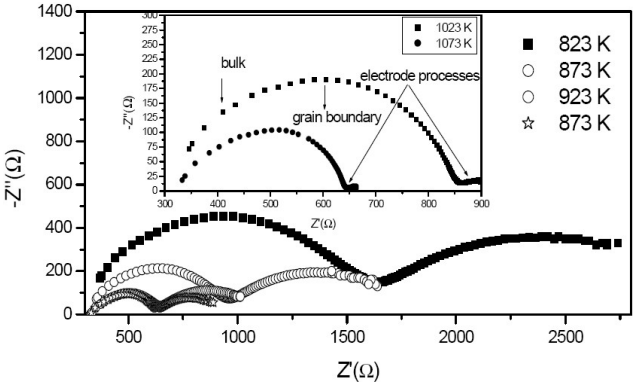

Figure 4 : Nyquist diagrams (-Z" vs. Z') of $La_{9.13}Bi_{0.2}(SiO_4)_6O_2$ oxyapatite

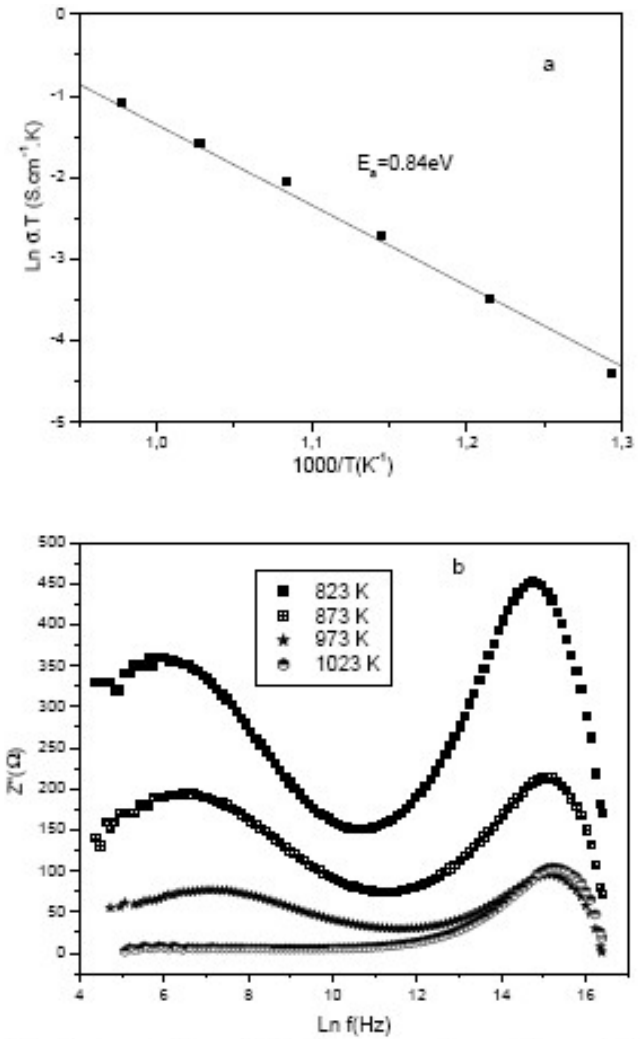

Figure 5 : (a) Arrhenius plot and (b) Frequency dependence of the imaginary parts (Z") of $La_{9.13}Bi_{0.2}(SiO_4)_6O_2$ oxyapatite

ture coefficient of resistance (NTCR) observed in semiconductors.

The conductivity (Figure 5a) is clearly thermally activated and follows the Arrhenius relation:

$$\sigma.T = A \exp(-E_a/kT)$$

where A is the pre-exponential factor (which is related to the effective number of mobile species), k Boltzmann's constant, *T* the temperature and E_a the activation energy.

The temperature dependence of total conductivity for $La_{9.13}Bi_{0.2}(SiO_4)_6O_2$ (Figure 5a), demonstrating a single conduction mechanism for the total conductivity, due to absence of apparent curvature in the plot.

Activation energy evaluated from the slope of Ln(σT) versus 1000/ T curve is 0.84eV. The $La_{9.13}Bi_{0.2}(SiO_4)_6O_2$ pellet sintered at 1523 K exhibited the ionic conductivity 1.4610^{-4} S.cm^{-1} at 923 K, which is better than obtained in the stoichiometric sample $Ba_2La_4Bi_4(SiO_4)_6O_2$ (σ=1.37 10^{-5})[17]. But, it is lower than 2.4 10^{-4} S. cm^{-1} reported for the $La_8Bi_2(SiO_4)_6O_3$ electrolyte at the same temperature[18]. Indeed, the non-stoichiometric (cation vacancies or oxygen excess) apatites show much higher conductivity than the fully stoichiometric (both cations and oxygen) apatites. This phenomenon is due to the fact that the oxygen ion migration in the fully stoichiometric apatites is via a vacancy mechanism, while for the non-stoichiometric ones is via an interstitial mechanism[19].

Figure 5b shows the variation of the imaginary part of impedance (Z") with frequency at different temperatures. The peak at lower frequency event has been related to bulk while the higher frequency event has been related to grain boundary. The plots show that the Z" values reach a maximum (Z''_{max}) and the value of Z''_{max} shifts to higher frequencies with increasing temperature, indicating that the net relaxation time is decreasing with the temperature increase. But some peaks have not been found at high temperatures (Te≥1023 K) which indicates a negligible of bulk contribution. The significant broadening of the peaks with rising temperature suggests the presence of a temperature-dependent electrical relaxation phenomenon in the sample.

The asymmetric broadening of the peaks suggests the presence of electrical process in the material with a spread of relaxation time[20,21].

CONCLUSION

$La_{9.13}Bi_{0.2}(SiO_4)_6O_2$ oxyapatite has been prepared by solid state reaction at high temperature. XRD confirmed the formation of oxyapatite phase crystallizing in the hexagonal system (space group $P6_3$ (173)). FTIR and Raman sectroscopies confirmed the formation of isolated SiO_4 groups. SEM-EDS results confirm the formation of composition of bismuth lanthanum silicate apatite.

The analysis of electrical properties indicates that the material exhibits (a) conduction due to bulk and grain boundary effects, (b) negative temperature coefficient of resistance (NTCR)-type behavior usually found in semiconductors and (c) temperature-depen-

dent relaxation phenomena. The total conductivity and the activation energy at 973 K are 1.4610^{-4} $S.cm^{-1}$ and 0.84 eV, respectively.

ACKNOWLEDGMENTS

The authors would like to thank Gerard PANCZER, Professor at the University Claude Bernard Lyon I, for his invaluable assistance in Raman spectra acquisition.

REFERENCES

[1] S.Nakayama, T.Kageyama, H.Aono, Y.Sadaoka; J.Mater.Chem., **5**, 1801 **(1995)**.
[2] E.J.Abram, D.C.Sinclair, A.R.West; J.Mater.Chem., **11**, 1978 **(2001)**.
[3] J.E.H.Sansom, D.Richings, P.R.Slater; Solid State Ionics, **139**, 205 **(2001)**.
[4] E.Kendrick, K.S.Knight, P.R.Slater; Mater.Res. Bull., **44**, 1806 **(2009)**.
[5] M.Santos, C.Alves, F.A.C.Oliveira, T.Marcelo, J.Mascarenhas, J.V.Fernandes, B.Trindade; Ceram.Int., **38**, 6151 **(2012)**.
[6] J.Xiang, Z.G.Liu, J.H.Ouyang, Y.Zhou, F.Y.Yan; Ceram.Int., **39**, 4847 **(2013)**.
[7] A.Mineshige, T.Nakao, M.Kobune, T.Yazawa, H.Yoshioka; Solid State Ionics, **179**, 1009 **(2008)**.
[8] T.Nakao, A.Mineshige, M.Kobune, T.Yazawa, H.Yoshioka; Solid State Ionics, **179**, 1567 **(2008)**.
[9] N.Lakshminarasimhan, U.V.Varadaraju; J.Solid State Chem., **178**, 3284 **(2005)**.
[10] K.Boughzala, E.Ben Salem, A.Ben Chrifa, E.Gaudin, K.Bouzouita; Mater.Res.Bull., **42**, 1221 **(2007)**.
[11] R.El Ouenzerfi, C.Goutaudier, G.Panczer, B.Moine, M.T.Cohen-Adad, M.Trabelsi-Ayedi, N.Kbir-Ariguib; Solid State Ionics, **156**, 209 **(2003)**.
[12] B.O.Fowler; Inorg.Chem., **13**, 194 **(1974)**.
[13] R.E.Rodriguez, A.F.Fuentes, M.Maczka, J.Hanuza, K.Boulahya, U.Amador; J.Solid State Chem., **179**, 522 **(2006)**.
[14] G.Lucazeau, N.Sergent, T.Pagnier, A.Shaula, V.Kharton, F.M.B.Marques; J.Raman Spectrosc., **38**, 21 **(2007)**.
[15] A.Orera, E.Kendrick, D.C.Apperley, V.M.Orera, P.R.Slater; Dalton Trans., **39**, 5296 **(2008)**.
[16] L.Zhang, H.Quan He, H.Wu, C.Li, S.P.Jiang; Int.J.Hydrogen Energy., **36**, 6862 **(2011)**.
[17] M.Abbassi, R.Ternane, I.Sobrados, A.Madani, M.Trabelsi-Ayadi, J.Sanz; Ceram.Int., **39**, 9215 **(2013)**.
[18] D.Y.Kim, S.G.Lee; Mater.Res.Bull., **47**, 2856 **(2012)**.
[19] J.R.Tolchard, M.S.Islam, P.R.Slater; J.Mater.Chem., **13**, 1956 **(2003)**.
[20] R.Bharati, R.A.Singh, B.M.Wanklyn; J.Mat.Sci., **16**, 775 **(1981)**.
[21] K.S.Rao, P.M.Krishna, D.M.Prasad; Phys.Status Solidi (B), **244**, 2267 **(2007)**.